Calibration and experiment of the discrete element parameters of watermelon seeds

Yong Chen[1†], Junwu He[1†], Xing Yu[2], Hao Ma[3], Shengsheng Wang[3*], Xiuli Zhang[1], Xinyu Ji[1], Xiaochan Liu[1]

(1. *College of Mechanical and Electrical Engineering, Henan Agricultural University, Zhengzhou 450002, China*;
2. *Yellow River Institute of Hydraulic Research, Yellow River Conservancy Commission, Zhengzhou 450003, China*;
3. *College of Agricultural equipment engineering, Henan University of Science and Technology, Luoyang 471003, Henan, China*)

Abstract: As important factors in discrete elements, the physical parameters of watermelon seeds play a pivotal role in discrete element method. To obtain the discrete element parameters of watermelon seeds and improve the accuracy of the discrete element model, through a combination of actual and simulation tests, this research has calibrated the seeds' physical and contact parameters with the seed metering device. Employing the Plackett-Burman experiment, this study has identified three critical factors affecting the stacking angle: the static and rolling friction coefficients between seeds, and the collision recovery coefficient between seeds and plexiglass. Using the steepest-climbing design and Box-Behnken response surface analysis, this research has optimized these factors to values of 0.716, 0.051, and 0.787, achieving a calibration error of just 2.60%. Verification with an air suction precision seed metering device confirmed the parameters' accuracy, with relative errors below 7.65%. The discrepancy between the simulation and actual test results, as measured by the qualified index error, is successfully reduced to below 4.38%. This study thus establishes a solid foundation for the structural optimization of air suction precision watermelon seed metering devices.

Keywords: watermelon seed, discrete element method, Plackett-Burman experiment, steepest-climbing design, Box-Behnken response surface analysis
DOI: 10.25165/j.ijabe.20251804.9570

Citation: Chen Y, He J W, Yu X, Ma H, Wang S S, Zhang X L, et al. Calibration and experiment of the discrete element parameters of watermelon seeds. Int J Agric & Biol Eng, 2025; 18(4): 26–37.

1 Introduction

Watermelon (*Citrullus lanatus*) seeds, known for their small, white-fleshed fruits with low sugar content, are predominantly cultivated on dry land or sandy dunes. These seeds are primarily harvested in the regions of Xinjiang and Gansu[1]. As agricultural technology advances, the adoption of mechanized precision sowing has become essential for boosting the profitability of watermelon seed farming. The efficiency of the seed metering device plays a pivotal role in improving the quality of sowing and, consequently, the overall yield and quality of the crop[2,3]. In recent years, researchers such as Yuan et al.[4], Zhang et al.[5], and Zhang et al.[6] have employed the discrete element method (DEM) and gas-solid coupling simulations, integrating EDEM and Fluent software, to optimize the performance of these devices.

The rapid advancement of computer technology has positioned the discrete element method (DEM) as a pivotal tool to analyze the kinematic characteristics of seed materials, with its applications now spanning the agricultural machinery sector. Given the inherent difficulty in directly and accurately obtaining material contact parameters, numerous scholars have proposed the innovative "virtual calibration" approach for material parameters using DEM. This method is designed to enhance the simulation and prediction of seed material kinematic behaviors. Barrios and Marcelo Tavares[7] pioneered the integration of multi-rigid-body dynamics simulations with DEM in the characterization of high-performance gas generators. Ghodki et al.[8] fine-tuned the parameters of the Hertz-Mindlin model for soybeans using the discrete element method (DEM). The experimental results obtained from the custom box device showed strong agreement with numerical simulations, thereby validating the computational model. This successful calibration significantly enhanced the reliability of subsequent DEM simulations for soybean harvesting equipment evaluation.

In recent years, researchers have conducted a variety of physical property tests on agricultural products and calibrated simulation parameters accordingly. Coetzee[9] determined the contact stiffness of corn through constrained compression tests and calibrated sliding and rolling friction coefficients. Liu et al.[10] created a discrete element method (DEM) model for rice seeds utilizing point cloud data. Tang et al.[11] utilized DEM to develop a discrete elemental model for corn seeds, which contributed valuable information for the design of a diverse seed metering device. Chen et al.[12] measured the friction coefficient using a reciprocating clamping friction coefficient meter and evaluated the coefficient of

Received date: 2024-11-25 **Accepted date:** 2025-06-04
Biographies: Yong Chen, PhD, Associate Professor, research interest: design and performance test of agricultural machinery, Email: chenyong@henau.edu.cn; **Junwu He**, MS candidate, research interest: mechanization design, Email: 15623803652@163.com; **Xing Yu**, PhD, Engineer, research interest: agricultural water-soil engineering, Email: yuxing1227@163.com; **Hao Ma**, PhD, Associate Professor, research interest: agricultural information technology, Email: mahao@haust.edu.cn; **Xiuli Zhang**, PhD, Professor, research interest: theory and method of agricultural equipment design, Email: zhangxiuli619@126.com; **Xinyu Ji**, Master candidate, research interest: mechanical principles, Email: 1977265546@qq.com; **Xiaochan Liu**, PhD, Lecturer, research interest: mechanization design, Email: liuxiaochan@henau.edu.cn.
†These authors contributed equally to this work.
***Corresponding author: Shengsheng Wang**, PhD, Associate Professor, research interest: design and performance test of agricultural machinery. College of Agricultural equipment engineering, Henan University of Science and Technology, Luoyang 471003, Henan, China. Tel: +86-13703491181, Email: ws@haust.edu.cn.

recovery with an inclined drop test, applying these parameters to DEM simulations to investigate the poured bulk density and reset angle for corn and wheat. Wang et al.[13] formulated discrete element models for maize seeds. Wu et al.[14] calibrated the physical properties of *peucedani radix* through the elevated hollow cylinder stacking test. Su et al.[15] applied the discrete element method (DEM) to investigate corn compression characteristics under uniaxial stress conditions. Through combined application of Plackett-Burman experimental design and response surface methodology, the study systematically examined the effects of key parameters including shear modulus, restitution coefficient, critical normal stress, and shear stress on rupture force and stiffness. Wang et al.[16] conducted an extensive investigation into the contact parameters of corn seeds with DEM, optimizing the angle of repose to determine the discrete element contact parameters. Li et al.[17] used the particle scaling method to calibrate the contact parameters for wheat flour. Lu et al.[18] proposed an ellipsoid modeling method to accurately simulate the movement of wheat seeds, demonstrating the ellipsoid model's superiority over the multi-sphere model in accuracy and robustness. Liu et al.[19] systematically calibrated discrete element parameters to accurately simulate straw flexibility. By integrating the Hertz-Mindlin contact model with a bonding particle approach in the EDEM software platform, the researchers developed an advanced double-layer straw bond model for discrete element analysis. Peng et al.[20] employed the discrete element software EDEM to address the uncalibrated contact parameters for peanut seedling membranes and the lack of precise simulation parameters for mechanized separation processes. Khatchatourian et al.[21] calibrated the principal material properties of soya beans and developed a three-dimensional model of soya bean flow. Li et al.[22] employed an integrated approach combining physical experiments with EDEM simulations. The researchers selected the Hertz-Mindlin model with JKR cohesion to calibrate the discrete element parameters for Protaetia brevitarsis larvae and frass mixture interactions. Xie et al.[23] investigated *Panax notoginseng* roots as their experimental subject, employing 3D scanning reverse modeling technology coupled with EDEM software to develop a discrete element model, subsequently conducting parallel physical and virtual experiments to calibrate the simulation parameters. Zhang et al.[24] proposed a calibration method for safflowers to obtain their physical parameter model. Fan et al.[25] proposed a comprehensive modeling methodology to describe wheat seeds with DEM. Zhao et al.[26] meticulously determined the physical characteristics of rice seeds, subsequently developing triaxial ellipsoidal particle models. These models were crafted using a multi-sphere technique, which provided a comprehensive representation of the seeds' geometry and behavior. Ding et al.[27] calibrated DEM parameters for *Cucurbita ficifolia* seeds and experimentally measured partial contact parameters of the seeds.

A multitude of research has utilized response surface methodology to examine various factors such as the static friction coefficient, rolling friction coefficient, restitution coefficient, particle size equivalence, and sphericity, with the stacking angle as the key response variable. These studies have leveraged the Plackett-Burman screening and the Box-Behnken experimental design. Among the factors investigated, the static friction coefficient, rolling friction coefficient, and restitution coefficient have been found to exert the most substantial influence on the stacking angle [28–31].

However, researchers in previous studies had not yet determined the specific parameters for watermelon seeds. Consequently, the current investigation involved measuring key physical properties of these seeds and constructing a discrete element model using point cloud technology and EDEM software. The parameters were meticulously analyzed and refined through a combination of the Plackett-Burman experiment, the steepest-climbing design, and Box-Behnken response surface methodology. The optimized experimental parameters were further analyzed using DEM simulation. The calibration results demonstrated a close agreement between the simulated and actual stacking angles, with a marginal error of 2.60%. Simulation of the air suction precision watermelon seed metering device revealed that all key dimensional parameters maintained errors below 7.65%, while the qualification index error was limited to 4.38%. The findings show that the calibrated parameters can effectively guide the design of the air suction precision watermelon seed metering device. Beyond optimizing the physical properties of watermelon seeds, this study establishes a theoretical foundation for enhancing the structural design of the air suction precision watermelon seed metering device.

2 Materials and methods

2.1 Calibration of physical parameters of watermelon seeds

2.1.1 The discrete element modeling method of watermelon seed

A random selection of 150 watermelon seeds (Jiuquan Golden Grain Agricultural Development Co., Ltd., Gansu, China), served as the basis for establishing a discrete element model using EDEM software. Given the seeds' irregular shapes, conventional modeling techniques like those in Solidworks or UG software were inadequate for accurately capturing the external contours. Thus, advanced 3D scanning processing was essential[32,33].

In this research, 25 seeds with comparable dimensions - length, width, and thickness - were chosen for scanning. An EinScan Pro 2X handheld blue laser 3D scanner (Shining 3D Tech Co., Ltd., Zhejiang, China) (scanning accuracy: 0.045 mm, scanning speed: 3×10^6 points/s, working distance: 300-500 mm) was employed for this purpose, as shown in Figure 1. This scanner was instrumental in capturing the seeds' external contours with precision. The resulting point cloud data were then imported into Geomagic Wrap 2021 software, where alignment commands and operations such as denoising were meticulously applied. Hole filling and peg elimination were also carefully executed to ensure data integrity. After these refinements, the data were exported to EDEM 2023 for the automated filling of particles, as shown in Figure 2. To achieve the discrete model of the watermelon seeds, the smoothing value for the filled particles was set to 5, and the minimum sphere radius was established at 0.5 mm. This configuration resulted in a detailed discrete model composed of 85 small spheres of varying sizes, accurately representing the watermelon seeds' complex geometry.

2.1.2 Poisson's ratio

Ten watermelon seeds were randomly selected for tensile testing using the ZQ-67 universal testing machine (Zhiqu Precision Instruments Co., Ltd., Dongguan, China), which can withstand a maximum load of 500 N. The seeds were securely fixed at both ends of the testing fixture. A stepping motor, operating at a controlled speed of 5 m/s, was used to gradually apply load to the seeds. The loading process was halted when initial signs of seed rupture were observed, with the deformation under tension being monitored and displayed on a computer client in real-time. Concurrently, a digital Vernier caliper (accuracy: 0.01 mm) was employed to meticulously measure the axial and lateral deformation of the seeds. This precise measurement technique ensured that the deformation data collected was both accurate and reliable, providing a comprehensive understanding of the seeds' response to tensile stress.

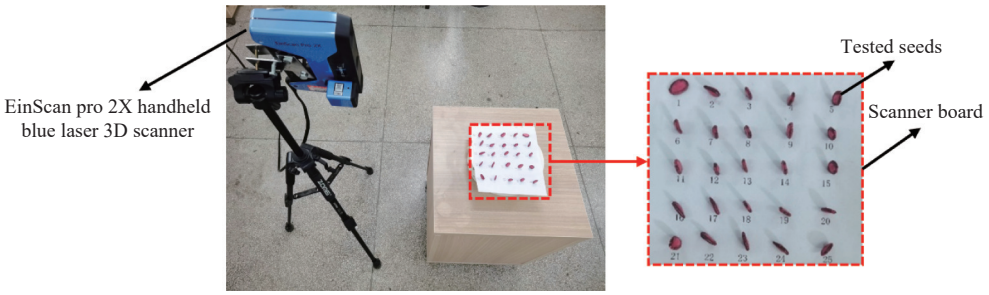

Figure 1 3D scanning working principle diagram

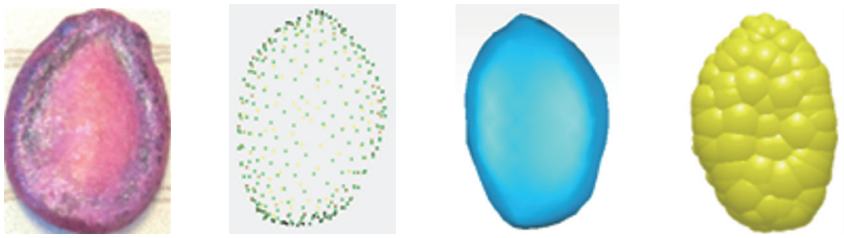

a. Raw image b. Point cloud processing c. Hole filling d. Discrete element model

Figure 2 Watermelon seeds particle and discrete element model process

The Poisson's ratio is calculated as:

$$\mu = -\frac{\varepsilon_x}{\varepsilon} = \frac{(b-B)/B}{(l-L')/L'} \quad (1)$$

where, ε_x and ε are the lateral strain and axial strain of watermelon seed, mm; b and B are the width of watermelon seed at rupture and before loading, mm; l and L' are the length of watermelon seed at rupture and before loading, mm.

2.1.3 Modulus of elasticity

ZQ-67 universal testing machine (Zhiqu Precision Instruments Co., Ltd., Dongguan, China) was selected for compression test, and the method was like the measurement of Poisson's ratio. The watermelon seed was fixed in the axial direction at the two ends of the gaps in the fixture. Then, the DS2 digital display push-pull tester (Dongguan Lixian Instrument Technology Co., Ltd., Dongguan, China) was used to measure the data. Within the universal testing machine, the operational velocity was configured at 5 m/s and the stroke length was set to 10 m. As listed in Table 1, the average working time was measured as 18.67 s, and the average load was 198.3 N.

The modulus of elasticity is calculated by the following equation:

$$E = \frac{\sigma}{\varepsilon'} \quad (2)$$

where, E is the modulus of elasticity, Pa; σ is the stress, N·m^{-2}; ε' is the strain, mm.

The stress σ and strain ε' were given by:

$$\sigma = \frac{F}{S} \quad (3)$$

$$\varepsilon' = \frac{l-L'}{L'} \quad (4)$$

where, F is the average load of ZQ-67 tensile strength universal testing machine at work, N; S is the force area of watermelon seed at work, m^2.

The average value of modulus of elasticity of watermelon seeds is calculated as 1.15×10^8 Pa.

The shear modulus is given by:

$$G = \frac{E}{2(1+\mu)} \quad (5)$$

where, G is the watermelon seed shear modulus, Pa.

The average value of watermelon seed shear modulus was calculated as 4.3×10^7 Pa. The simulation parameters for other materials are listed in Table 2.

Table 1 Results of compression test measurement of watermelon seed

Serial number	Working time/s	Working load/N	Stress/N·m^{-2}	Strain/mm
1	19.00	182.7	1.16×107	0.20
2	19.00	216.0	1.37×107	0.15
3	18.00	196.2	1.25×107	0.16
Mean	18.67	198.3	1.26×107	0.17

Table 2 Other material simulation parameters

Parameters	Number
Poisson's ratio of plexiglass sheet	0.32
Density of plexiglass sheet/kg·m^{-3}	1190
Plexiglass sheet shear modulus/Pa	1.2×10^9

3 Contact parameter calibration

3.1 The calibration of collision recovery coefficient

The coefficient of restitution, a key factor in discrete element modeling, represents the energy loss when watermelon seeds collide. This parameter is crucial for precisely simulating and analyzing the seeds' dynamic responses. In scenarios where collisions are not perfectly elastic, the restitution coefficient is calculated as the proportion of an object's post-collision velocity along the normal axis to its pre-collision velocity along the axis. This coefficient provides a quantitative measure of the conservation of momentum in the direction perpendicular to the surfaces of contact during the collision event[34]. In this study, the collision was categorized as an inelastic collision due to the energy loss during the collision[13].

Owing to the irregular shape of watermelon seeds, during inelastic collisions, the contact points and contact areas are subject to continuous alteration. This variability can induce intricate rotational and rolling motions, rendering the distribution of collision forces both complex and uneven. Consequently, the complexity and

uncertainty of the collision process are significantly heightened, ultimately compromising the accuracy of free-fall tests. Therefore, to measure more accurately, a flat plate collision device was designed by two plexiglass plates of the same size (L×W×T: 22×20×5 mm) bonded together by the special glue for acrylic plates, and a digital angle meter was used to form an inclination angle θ as 45°. Twenty watermelon seeds were randomly selected for the collision test, and the falling height of H_0 was set as 300 mm. To better observe the test, the height camera was used to record in detail the oblique throwing motion process of the seeds, and the collision effects of the most ideal 10 seeds were observed and selected frame by frame. The trajectory was measured and calculated accurately as shown in Figure 3.

The equation for the collision recovery coefficient is:

$$e = \frac{v_n'}{v_n} \tag{6}$$

where, e is the collision recovery coefficient; v_n' is the instantaneous velocity of the rebound post-collision of the watermelon seed, m/s; v_n is the instantaneous velocity of the watermelon seed pre-collision, m/s.

The velocity at which the watermelon seed approaches the material just before impact is:

$$v_n = v_0 \cos\theta' \tag{7}$$

$$v_0 = \sqrt{2gH_0} \tag{8}$$

where, v_0 is the free-fall velocity at the instant pre-collision, m/s; θ' is the angle formed between the normal to the collision surface at the point of contact and the direction of the seed's free fall, (°); H_0 is the height from which the seed is dropped, m; v_n is the normal approach velocity post-collision, m/s.

After the collision at point O, the watermelon seed was thrown downward obliquely.

The formula for determining the seed's instantaneous velocity in the normal direction following a collision is presented below:

$$v_n' = \sqrt{\left(v_x^2 + v_y^2\right)\cos\left(\beta + \arctan\frac{v_y}{v_x}\right)} \tag{9}$$

where, v_x is the post-collision velocity of the watermelon seed in the x-axis direction, m/s; v_y is the post-collision velocity in the y-axis direction, m/s.

The equation of v_x and v_y are calculated by the following equations:

$$v_x = \frac{L}{t} \tag{10}$$

$$v_y = \frac{H_1}{t} - \frac{gt}{2} \tag{11}$$

where, L is the horizontal distance of the lowest point when the watermelon seed is thrown obliquely, m; H_1 is the vertical distance of the lowest point when the seed is thrown obliquely, m.

This is obtained by substituting Equation (7) and (9) into Equation (6):

$$e = \frac{\sqrt{v_x^2 + v_y^2}\cos\left(\theta' + \arctan\frac{v_y^2}{g}\right)}{\sqrt{2gH_0\cos\theta'}} \tag{12}$$

The collision recovery coefficients of seed-plexiglass and seed-seed were calculated as 0.733 and 0.779, respectively.

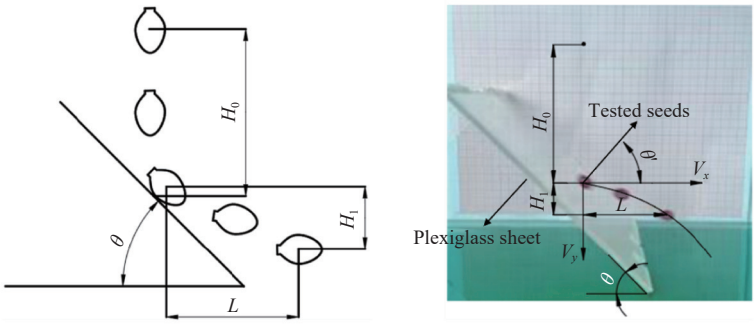

a. Simulation test b. Practicaltest

Figure 3 Calibration test of collision recovery coefficient of watermelon seeds

3.2 The calibration of static friction coefficient

A random selection of 10 watermelon seeds was used to ascertain the static friction coefficient, denoted as μ_s, employing the slant slip method. The experimental arrangement for this test is shown in Figure 4.

The inclined plane was equipped with a plexiglass sheet on which the watermelon seed was laid flat. As the angle of inclination was slowly raised, the seed began to slide downward. The plate remained stationary while the angle of inclination α was precisely measured using a digital inclinometer (Weidu Electronics Co., Ltd., Wenzhou, China). Figure 5a illustrates that the static friction angle between the seed and the plexiglass was recorded as 22.28°.

The seed-bearing platform was attached to the sloping surface employing a uniform method. Gradually increasing the slope's gradient triggered the seeds to descend. A digital inclinometer was subsequently used to ascertain the angle of inclination α. As depicted in Figure 5b, the angle of static friction between the seeds was found to be 34.94º.

The static friction coefficient equation is as follows:

$$\mu_s = \tan\alpha \tag{13}$$

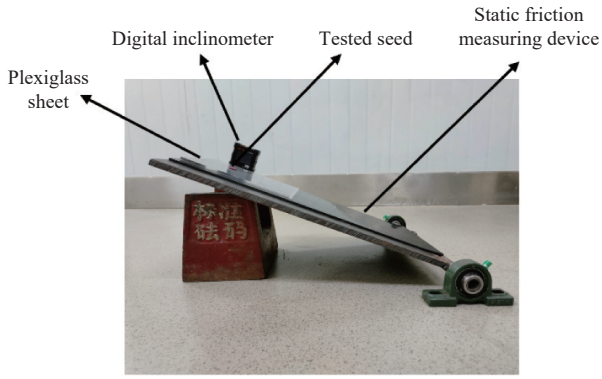

Figure 4 Device for determining the static friction coefficient between seed and plexiglass

where, μ_s is the static friction coefficient; α is the inclination angle, (°).

The average static friction coefficient between the seeds and the plexiglass was found to be 0.41, while the average coefficient among the seeds themselves was 0.7.

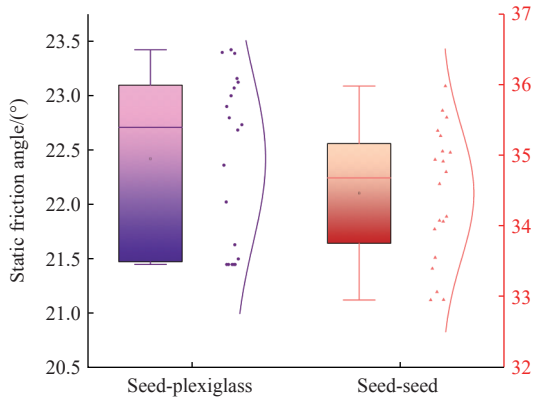

Figure 5 Distribution of the angle of static friction

The determination of the static friction coefficient between the seed and plexiglass was accomplished with EDEM software, which also facilitated the calibration of the collision recovery coefficient. The static friction coefficient was adjusted over an interval from 0.1 to 0.6. To reduce external influences, all additional contact parameters were standardized to zero. Each experiment was conducted five times and the mean value was taken as the result, and the data were then analyzed to establish a correlation between the angle of inclination and the static friction coefficient, as illustrated in Figure 6a.

The regression analysis indicated a coefficient of determination R^2 of 0.98 for the model, which is nearly perfect and indicates a strong fit. By substituting the measured inclination angle into the regression equation, the static friction coefficient μ_s was determined to be 0.44. The relative error against the experimental data was 7.31%, indicating a high degree of agreement between the simulation outcomes and the experimental findings. As a result, the static friction coefficient at the seed-plexiglass interface was confirmed to be 0.44.

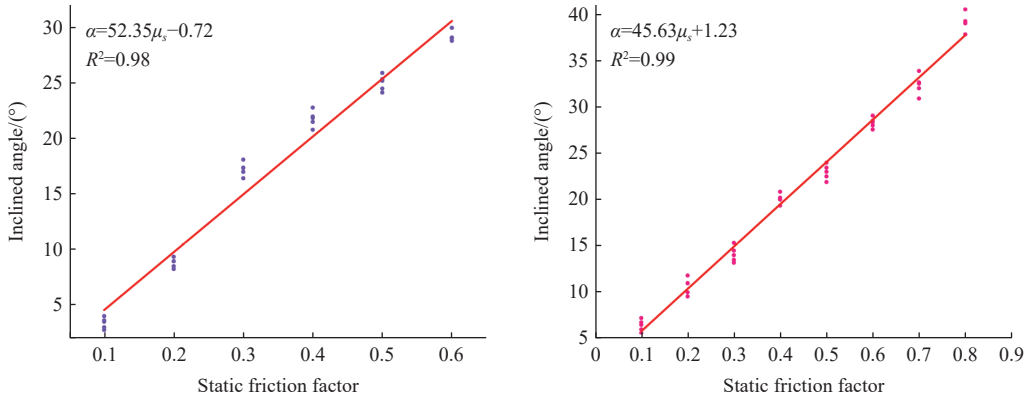

a. Seed-plexiglass b. Seed-seed

Figure 6 Fitting treatment of static friction coefficient and inclined angle

The method for calibrating the static friction coefficient between seeds is the same as the previously mentioned method for calibrating the static friction coefficient between seeds and plexiglass. The procedure involves performing simulations using EDEM software, incorporating a seed plate structure, setting its physical property parameters (Poisson's ratio, elastic modulus, and density), and then conducting the test. The static friction coefficient was adjusted over a broader range from 0.1 to 0.8, increasing by 0.1 each time. All other contact parameters were zeroed out. Each test configuration was executed five times to determine an average, as depicted in Figure 6b. The fitting equation's coefficient of determination, R^2, was 0.99, nearly perfect. Using the actual measured angle of inclination in the fitting equation yielded a static friction coefficient μ_s of 0.74. The relative error against the experimental value was 5.71%, suggesting a high concordance between the calibrated simulation and the empirical measurements. Consequently, the static friction coefficient for the seed-seed interaction was established at 0.74.

3.3 The calibration of rolling friction coefficient

The rolling friction coefficient is affected by various factors, including the seed's mass, its shape, and the characteristics of the surfaces in contact. The slant rolling method was employed to ascertain the rolling friction coefficient μ_m for both seed-seed and seed-plexiglass interactions. To minimize error, a selection of 10 watermelon seeds with high sphericity φ and uniform particle size D was made. The seeds were positioned on an inclined plane and allowed to roll freely from the rest. The horizontal displacement S_m was measured upon reaching the complete stop. As illustrated in Figure 7, the measured average horizontal rolling distances for the seed-plexiglass and seed-seed contacts were 7.44 cm and 6.08 cm, respectively.

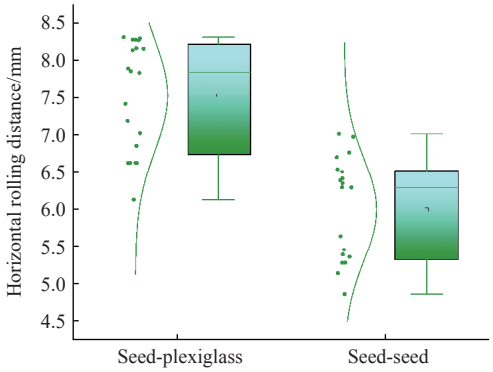

Figure 7 Distribution of horizontal rolling distance

EDEM software was utilized to ascertain the rolling friction coefficients for both the seed-plexiglass and seed-seed contacts. The collision recovery coefficient and static friction coefficient,

which had been previously calibrated, were applied in these tests. The rolling friction coefficient was varied from 0.01 to 0.08, with increments of 0.01 for each trial. To minimize external influences, all other contact parameters were standardized to zero. Each experiment was repeated five times to determine an average value, and the results were based on the relationship between the rolling distance and the rolling friction coefficient, as shown in Figure 8.

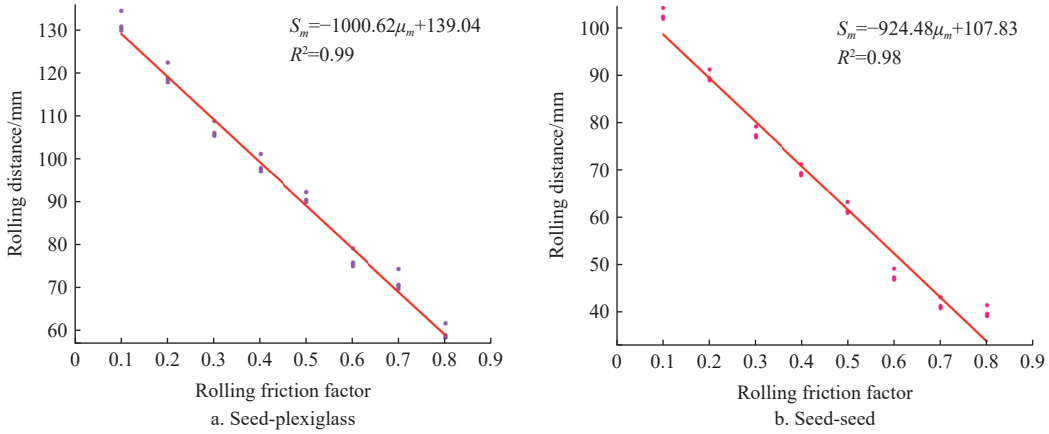

Figure 8 Fitting treatment of rolling distance and rolling friction coefficient

The regression analysis yielded high confidence R^2 values of 0.99 and 0.98 for the equations fitted to the data. By substituting the actual rolling distances S_m into the equations, the rolling friction coefficients μ_m were calculated as 0.065 and 0.051 for seed-plexiglass and seed-seed interactions, respectively. The simulation experiments, each conducted five times for the purpose of averaging, resulted in rolling distances of 7.02 cm and 5.89 cm, with respective relative errors of 5.65% and 3.13% when compared to the empirical measurements. These results indicate a high degree of correspondence between the calibrated simulation outcomes and the actual experimental data. Consequently, the rolling friction coefficients for the interfaces between the seeds and plexiglass, as well as between the seeds themselves, were confirmed to be 0.065 and 0.051, respectively.

4 Stacking experiment

4.1 Physical stacking angle measurements

The stacking angle of bulk materials, as an important index of material dispersal properties and friction characteristics, is affected by multiple factors such as the characteristics of the particles and the environment. Prior to conducting the experiment, a glass cylinder with a specific size specification (outer diameter: 73 mm, inner diameter: 30 mm, wall thickness: 2.5 mm, length: 260 mm) without top and bottom was selected. The experiment was carried out on a miniature iron stand, as shown in Figure 9, where a square plexiglass plate was placed at the base of the stand for supporting and observing the material stacking process to ensure the stability and accuracy of the operation. The cylinder was fixed on the iron frame table and clamped by a universal claw clamp to ensure that it would not wobble or move during the experiment. The cylindrical vessel was brimming with watermelon seeds. As the vessel was gently elevated, the seeds cascaded downwards, gathering into a conical heap under the influence of gravity. Upon reaching equilibrium, the incline of this heap relative to the horizontal plane was recognized as the repose angle.

To ensure measurement accuracy, a high-definition camera was utilized to capture clear images of the stacking angle formation. The acquired images were subsequently processed through a MATLAB involving grayscale conversion, binarization, noise reduction, and contour extraction, as illustrated in Figure 10. The gradient of the derived regression line was converted into the stacking angle of watermelon seeds. This experimental process was systematically repeated five times to establish a reliable average stacking angle of 28.64° for watermelon seeds. The simulation determined value was then incorporated in EDEM software, as shown in Figure 11. The simulation results yielded a stacking angle of 26.85°, demonstrating a 6.25% relative error compared to the experimental measurements. This close agreement between experimental and simulated values validates the robustness of both the measurement methodology and the simulation approach.

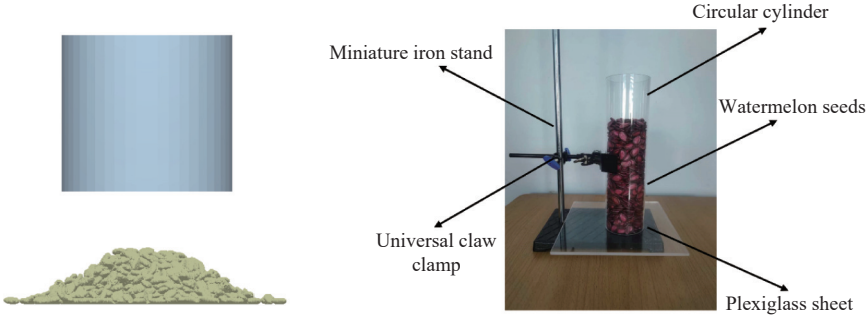

Figure 9 Assessment of the stacking angle

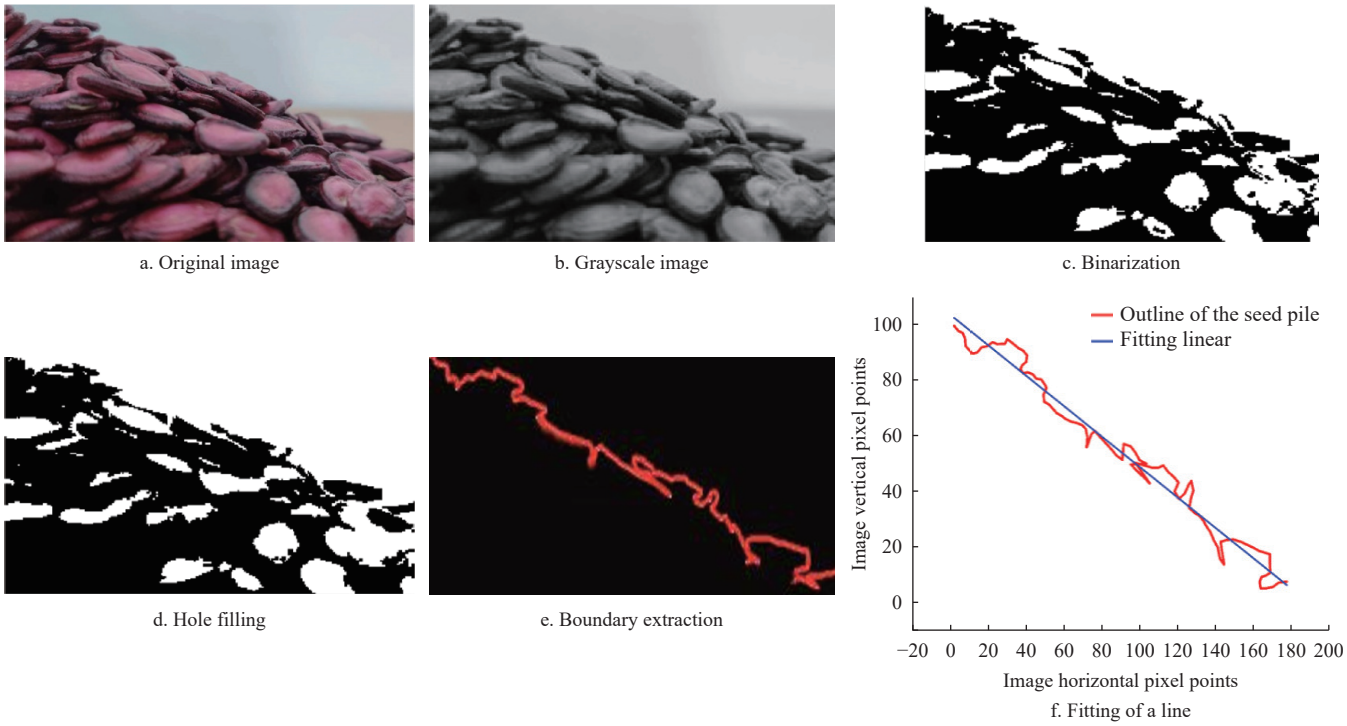

Figure 10 Physical stacking angle image procession

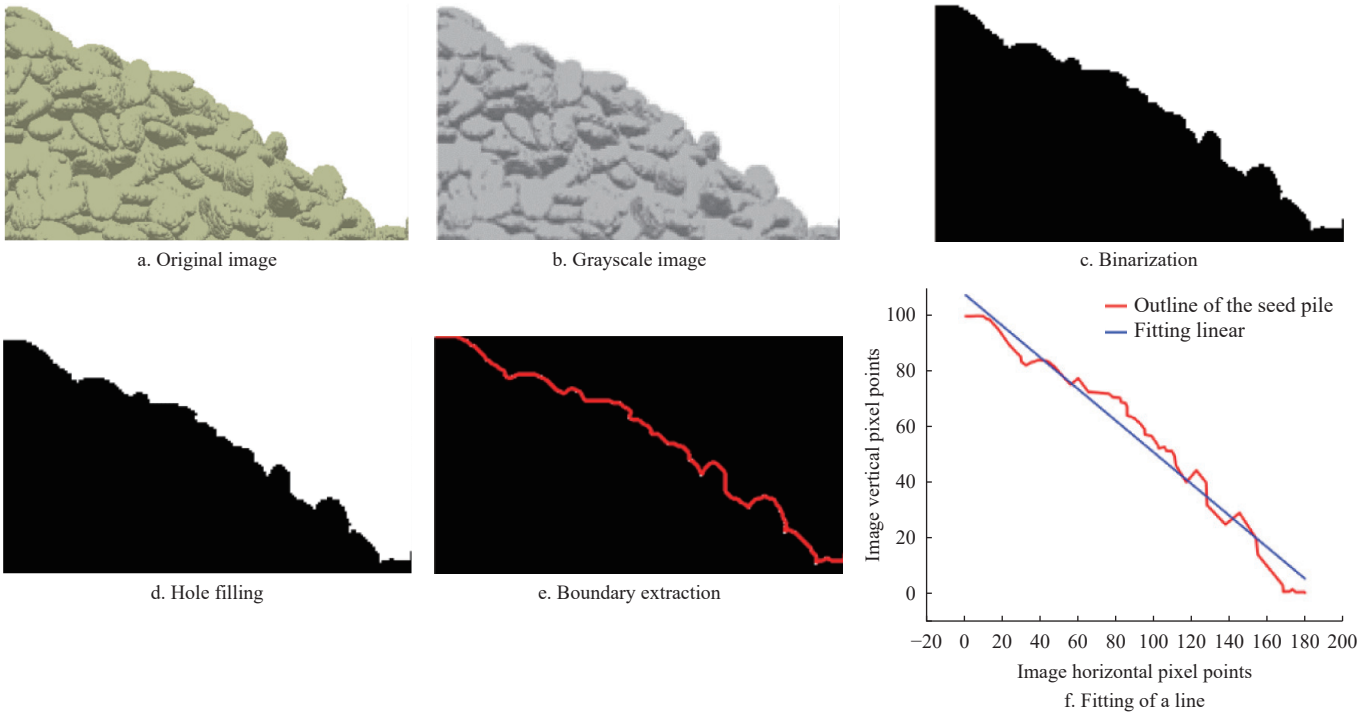

Figure 11 Simulation of stacking angle image procession

4.2 Tested method design

4.2.1 Plackett-Burman experiment

To identify the key factors significantly influencing the stacking angle, a Plackett-Burman design experiment was conducted with six critical factors (W-W S, W-P S, W-W R, W-P R, W-W T, and W-P T), while three additional dummy variables were incorporated for error analysis. The stacking angle served as the response variable, with each factor assigned two levels: high and low, coded as 1 and –1, respectively. The complete list of parameters for the Plackett-Burman experiment is detailed in Table 3. Following each set of simulations, images of the stacking angles were captured. These simulated angles were then measured and adjusted to approximate the tangent values.

Table 3 Factors and levels in the Plackett-Burman design experiment

Parameters	Level	
	–1	1
Static friction coefficient of watermelon-watermelon (W-W S)	0.640	0.840
Static friction coefficient of watermelon-plexiglass (W-P S)	0.340	0.540
Rolling friction coefficient of watermelon-watermelon (W-W R)	0.031	0.151
Rolling friction coefficient of watermelon-plexiglass (W-P R)	0.045	0.085
Restitution coefficient of watermelon-watermelon (W-W T)	0.678	0.880
Restitution coefficient of watermelon-plexiglass (W-P T)	0.616	0.850

4.2.2 The steepest-climbing design

Based on the Plackett-Burman experiment, three key parameters were determined: the static friction coefficient between watermelon-watermelon, the rolling friction coefficient between watermelon-watermelon, and the restitution coefficient of watermelon-plexiglass. To develop an effective response surface model, the steepest-climbing design was utilized to rapidly and efficiently narrow down the optimal parameter range for these significant factors. The trajectory of the steepest-climbing design was guided by the positive or negative influence exerted by the significant factors. The magnitude of each step in the ascent was calibrated based on the effect size of the respective factor, while the levels of the less significant factors were maintained at their average values throughout the experimentation.

4.2.3 Box-Behnken response surface analysis

After arriving at the optimal response area using the steepest-climbing design, the Box-Behnken method was then applied for response surface analysis. For this design, three levels of the significant factors were chosen, and the less influential factors were adjusted to their median values in the experimental setup. Utilizing the regression equation, a three-dimensional response surface plot was generated to visualize the analysis. This method aided in predicting the actual stacking angle and confirming the most favorable set of parameters for simulating watermelon seed.

5 Results and discussion

5.1 Findings from the Plackett-Burman experiment

The outcomes of the Plackett-Burman experiment are presented in Table 4 and were analyzed using ANOVA with the Design-Expert software. As per the data in Table 5, the model's p-value was 0.0315 (less than 0.05), signifying that the regression model's impact was statistically significant. The experiment identified three factors with a substantial influence on the stacking angle: the static friction coefficient between watermelon seeds (p=0.0045), the collision recovery coefficient between watermelon seeds and plexiglass (p=0.0320), and the rolling friction coefficient between watermelon seeds (p=0.0451). Other factors did not significantly affect the stacking angle (p>0.05). Consequently, three influential factors were selected for the steepest-climbing design. The Pareto chart in Figure 12 illustrates the positive and negative impacts of these factors on the stacking angle. It was observed that the static

Table 4 Outcomes from the Plackett-Burman experiment

Coding	A	B	C	D	E	F	G	H	J	Stacking angle/(°)
1	–1	–1	–1	–1	–1	–1	–1	–1	1	22.19
2	1	–1	1	1	1	–1	1	1	1	36.51
3	1	1	–1	1	1	1	1	1	–1	27.64
4	–1	–1	1	–1	1	1	–1	–1	–1	28.77
5	1	1	1	–1	–1	–1	1	1	–1	50.52
6	1	–1	–1	–1	1	–1	–1	1	1	47.06
7	–1	–1	–1	1	–1	–1	–1	–1	–1	14.27
8	–1	1	–1	1	1	–1	1	–1	–1	30.76
9	1	1	–1	–1	–1	1	–1	1	1	35.09
10	–1	1	1	1	–1	–1	1	–1	1	28.29
11	1	–1	1	1	–1	1	–1	–1	1	40.83
12	–1	1	1	–1	1	1	–1	1	–1	27.31

Note: A: W-W S; B: W-P S; C: W-W R; D: W-P R; E: W-W T; F: W-P T; G, H, J: Virtual parameter.

Table 5 Plackett-Burman experiment parameter significance assessment

Source	Sum of squares	*df*	Mean square	*F*-value	*p*-value
Model	1047.99	6	174.67	8.07	0.0315*
W-W S	717.86	1	717.86	33.16	0.0045**
W-P S	2.20	1	2.20	0.1017	0.7657
W-W R	179.44	1	179.44	8.29	0.0451*
W-P R	20.14	1	20.14	0.9300	0.3895
W-W T	35.07	1	35.07	1.62	0.2721
W-P T	225.88	1	225.88	10.43	0.0320*
Residual	86.60	4	21.65	-	-
Cor total	1134.59	10	-	-	-

Note: * shows this model is significant (0.01<p<0.05); ** shows this model is highly significant (p<0.01).

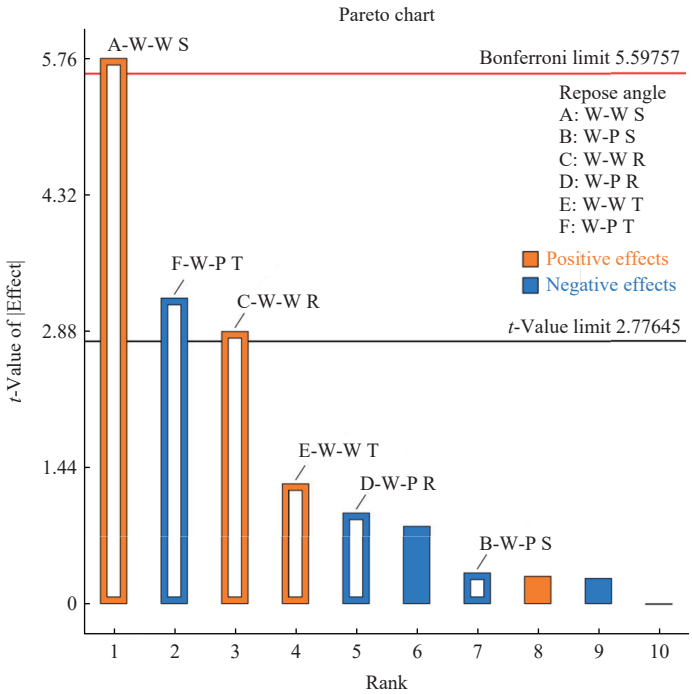

Figure 12 Positive and negative impact of Pareto chart

and rolling friction coefficients between watermelon seeds positively influenced the stacking angle, whereas the collision recovery coefficient between watermelon seeds and plexiglass had a negative impact. Thus, an increasing trend was noted for the friction coefficients of watermelon seeds, while the collision recovery coefficient showed a decreasing trend.

5.2 Determining the optimal independent variables region through steepest-climbing design

The results from the steepest-climbing design, as influenced by the three significant factors and their respective positive and negative effects identified in the Plackett-Burman experiment, are summarized in Table 6. It is noticeable that the stacking angle's error first diminishes and then subsequently rises. Particularly, the test with the lowest relative error was identified as the third one conducted. As a result, Test 3 was selected as the central point at a moderate level, with Tests 2 and 4 being designated to represent the lower and upper levels, respectively, for the subsequent Box-Behnken response surface analysis.

Table 6 Results of the steepest-climbing design

Coding	Factors			Angle of repose/(°)	Relative error/%
	W-W S	W-W R	W-P T		
1	0.64	0.03	0.86	21.23	25.90
2	0.68	0.05	0.82	25.21	12.01
3	0.72	0.07	0.78	29.79	3.980
4	0.76	0.09	0.74	33.24	16.02
5	0.80	0.11	0.70	35.80	24.96
6	0.84	0.13	0.66	40.11	40.00
7	0.88	0.15	0.62	42.52	48.41

5.3 Box-Behnken response surface analysis to determine material parameters

A composite design was implemented, focusing on the three key factors identified through both the Plackett-Burman experiment and the steepest-climbing design[27,31]. The findings from the Box-Behnken response surface analysis are presented in Table 7.

The regression model is given by:

$$\begin{aligned}\delta =& 6306.1-8789.8\times(W-WS)-4695.7\times(W-WR)-\\ & 7865.3\times(W-PT)+931.3\times(W-WS)\times(W-WR)-\\ & 378.1\times(W-WS)\times(W-PT)+4871.88\times(W-WR)\times(W-\\ & PT)+6358.88\times(W-WS)^2+3345.74\times(W-WR)^2+\\ & 5060.44\times(W-PT)^2 \end{aligned} \quad (14)$$

Referencing Table 8, the p-value associated with the regression model was 0.0063, which is below the 0.01 threshold, indicating that the model is statistically significant. The p-value for the lack of fit was 0.0739, exceeding the 0.05 level, which implies that the deviation from normality in the model's error term and the actual fit are not significant, and no other influential factors were identified. The determination coefficient, R^2, for the regression equation was 0.98, signifying an excellent fit and the model's capability to precisely depict the correlation between the experimental variables and the relative error in the stacking angle. As a result, the model is considered dependable for the analysis and prediction of the stacking angle in watermelon seeds.

The results of the analyses revealed that the static friction coefficient between seeds had a substantial influence on the stacking angle. Additionally, the rolling friction coefficient between seeds and the collision recovery coefficient between seeds and plexiglass were also found to be significant factors. After processing the data, the response surface is illustrated in Figure 13. The stacking angle's relative error was found to be at its lowest when the static friction coefficient of seed-seed, rolling friction coefficient of seed-seed, and the collision recovery coefficient of seed-plexiglass interactions were within the intervals of 0.70 to 0.74, 0.06 to 0.08, and 0.76 to 0.80, respectively. Utilizing the Design-Expert software's point prediction optimization module, several optimal parameter combinations were identified that closely approached the target value, as illustrated in Figure 14. A relative error of 2.60% was obtained with the following parameter values: the static friction coefficient between seeds was 0.716, the rolling friction coefficient between seeds was 0.051, and the collision recovery coefficient between seeds and plexiglass was 0.787. The other parameters were adjusted based on experimental findings: the static friction coefficient for the interaction between seeds and plexiglass was set to 0.44, the rolling friction coefficient for the same interaction was 0.065, and the collision recovery coefficient between seeds was 0.779.

Table 7 Design and results of the Box-Behnken response surface analysis

Run	*A*	*B*	*C*	Relative error/%
1	0.72	0.09	0.78	10.82
2	0.76	0.07	0.74	28.37
3	0.68	0.07	0.82	21.02
4	0.72	0.09	0.82	32.01
5	0.72	0.07	0.78	8.62
6	0.68	0.05	0.78	6.56
7	0.76	0.05	0.78	18.85
8	0.68	0.09	0.78	15.01
9	0.76	0.07	0.82	27.98
10	0.72	0.09	0.74	9.39
11	0.72	0.05	0.74	6.98
12	0.68	0.07	0.74	18.99
13	0.76	0.09	0.78	30.28
14	0.72	0.07	0.78	6.47
15	0.72	0.05	0.82	14.01
16	0.72	0.07	0.78	5.99
17	0.72	0.07	0.78	3.57

Note: A: W-W S; B: W-W R; C: W-P T.

Table 8 ANOVA of Box-Behnken test

Source	Sum of squares	*df*	Mean square	*F*-value	*P*-value
Model	1312.70	9	145.86	7.90	0.0063**
A	240.90	1	240.90	13.04	0.0086**
B	208.24	1	208.24	11.27	0.0121*
C	122.38	1	122.38	6.62	0.0368*
AB	2.22	1	2.22	0.1202	0.7390
AC	1.46	1	1.46	0.0793	0.7865
BC	60.76	1	60.76	3.29	0.1126
A^2	433.77	1	433.77	23.48	0.0019**
B^2	7.51	1	7.51	0.4063	0.5442
C^2	274.71	1	274.71	14.87	0.0062**
Residual	129.32	7	18.47	-	-
Lack of fit	116.44	4	29.11	6.78	0.0739
Pure error	12.88	3	4.29	-	-
Cor total	1442.02	16	-	-	-

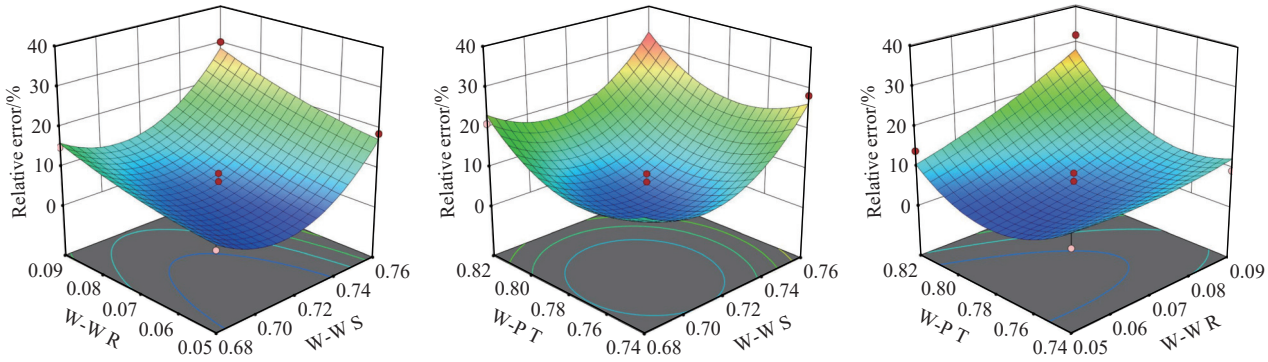

Figure 13 Effects of test factors on stacking angle response surfaces

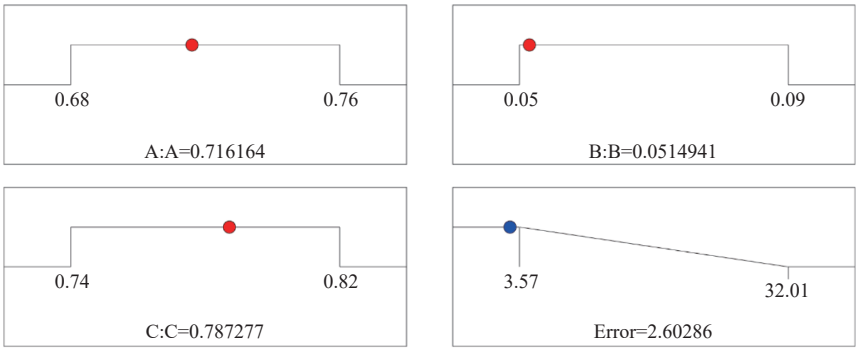

Figure 14 Optimal parameter combination results

5.4 Verification test

Selected calibrated simulation parameters were employed for experimental verification using an air suction precision watermelon seed metering device. A random sample of 500 watermelon seeds was poured from a plexiglass seed inlet into the inner chamber of the metering device, as depicted in Figure 15. Once the seeds achieved static equilibrium within the device and ceased self-movement, key distances (H_1: vertical distance from the outermost seed boundary at the inlet to the metering plate's horizontal centerline; H_2: distance from the seed edge contour intersection with the left observation window line to the metering plate's horizontal centerline; H_3: distance from the seed edge contour to the right observation window line, measured to the metering plate's horizontal centerline) were measured to assess the spatial distribution characteristics. In the seeds' stable configuration, the upper boundary outline and three critical dimensions (L_1: vertical distance from the seed's left edge to the lower edge of the transparent observation window; L_2: distance from the seed's right edge to the same lower edge; L_3: fixed horizontal length of the observation window) defined an irregularly shaped, approximately trapezoidal region (as shown in Figure 16). The vertical edge lengths L_3 and L_4 of the transparent window were set at 47.26 mm and 56.49 mm, respectively. The density of the watermelon seeds' accumulation at the bottom of the metering device was quantified using the following equations:

$$r = \frac{S_1}{S} \tag{15}$$

$$S_1 = \frac{(L_1 + L_2) L_3}{2} \tag{16}$$

$$S = L_3 L_4 \tag{17}$$

where, r is the degree of dense accumulation of the watermelon seed population, %; S_1 is the contact cross-sectional area, mm^2; S_2 is the entire area of the transparent window, mm^2; L_1 is the vertical distance from the left boundary of the seed population to the lower edge of the observation window, mm; L_2 is the vertical distance from the right boundary of the population to the lower edge of the observation window, mm; L_3 is the fixed length of the horizontal side of the transparent observation window, mm; L_4 is the distance of the vertical edge of the transparent window, mm.

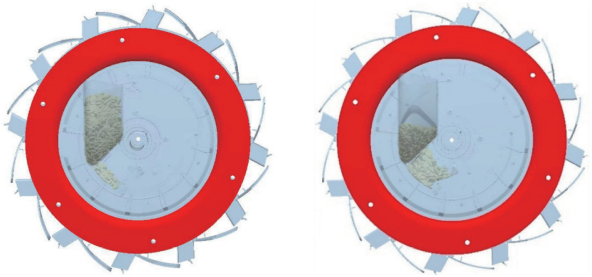

a. Pre-calibration simulation stacking test

b. Post-calibration simulation stacking test

Figure 15 Physical and simulation tests before and after calibration of the seed metering device

Separate measurements and statistical analyses were conducted for both the simulated and physical experiments, with the outcomes detailed in Table 9. The results demonstrated that the simulation discrepancies for the critical dimensions H_1, H_2, H_3, L_1, L_2, and the ratio of the stacked cross-sectional area r were all within 7.65%. This indicated that the seed flow was more streamlined post-calibration, and the contact parameters of the seed-filled model more closely resembled the actual contact parameters than before calibration.

To ascertain the accuracy of the calibration parameters more rigorously, a comparative study was carried out between the actual seed metering mass of the seed metering device and its simulated equivalent under the set simulation parameters, as depicted in Figure 17. The results showed that under a constant negative pressure of 5.5 kPa and a rotational speed between 35-55 r/min, the deviation between the actual qualified index and the simulated

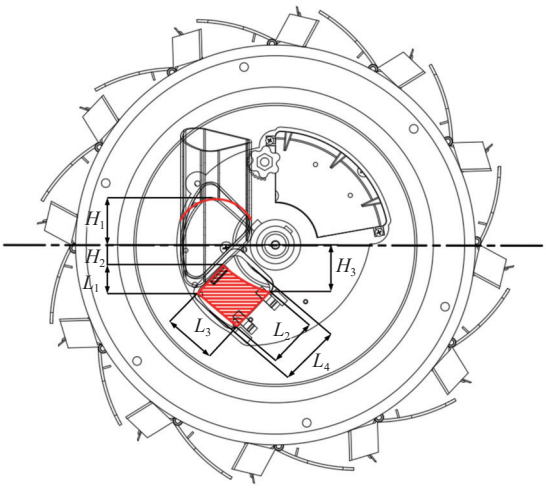

Figure 16 Schematic diagram of key feature dimensions of the seed metering device

qualified index stayed within an acceptable range of 3.97%. Likewise, when the rotational speed was fixed at 45 r/min and the negative pressure was adjusted from 5 to 7 kPa, the discrepancy between the actual qualified index and the simulated qualified index was within 4.38%. These findings confirmed the high precision of the DEM modeling method and the simulation parameters established for watermelon seeds.

Table 9 Comparison of key characteristic size parameters of simulated and physical test populations

Parameters	Simulation measurements/mm	Actual measured value/mm	Relative error/%
H_1	38.32	40.00	4.20
H_2	13.86	14.41	3.82
H_3	37.87	40.36	6.17
L_1	23.61	24.25	2.64
L_2	45.29	49.04	7.65
r	0.61	0.65	6.15

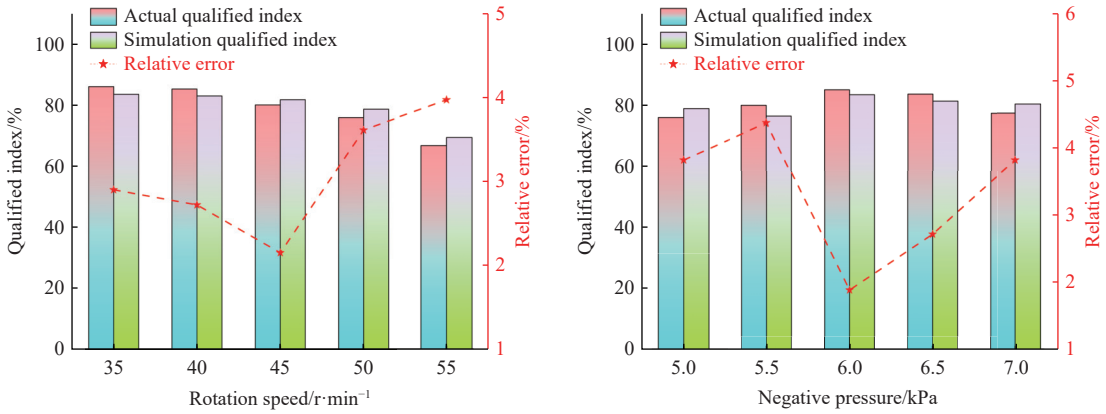

Note: a. The analysis of the variance was conducted under conditions where a constant negative pressure of 5.5 kPa was applied, and the rotational speed was varied between 35-55 r/min (as shown in *x*-axis). b. The analysis focused on the discrepancies under conditions where the rotational speed was fixed at 45 r/min and the negative pressure was adjusted within the range of 5 to 7 kPa (as shown in *x*-axis).

Figure 17 Comparative analysis of actual seed metering results and simulated seed metering results

6 Conclusions

1) The study focused on watermelon seeds as the subject of investigation. Employing 3D scanning technology and point cloud processing methods, the external contours of the seeds were captured. Following encapsulation, the Hertz-Mindlin (no-slip) contact model and an auto-filling approach within EDEM software were utilized to construct a discrete metamodel of the watermelon seeds.

2) The fundamental parameters for interactions between the seeds and plexiglass, as well as between seed and seed, were ascertained through a blend of laboratory bench tests and simulation experiments. A stacking test was performed on the watermelon seeds, yielding an actual stacking angle measurement of 28.64°. The Plackett-Burman experimental design was employed to identify the three most influential factors on the watermelon seed population, which were found to be the static friction coefficient between watermelon seeds, the rolling friction coefficient between watermelon seeds, and the collision recovery coefficient between watermelon seeds and plexiglass.

3) Through the stacking test simulation, a thorough examination of the three key factors was performed using the steepest-climbing design and the Box-Behnken response surface analysis. The findings indicated that the regression models were highly fitted, precise, and reliable, effectively capturing the relationship between the experimental variables and the relative error in the stacking angle. Consequently, the most favorable simulation parameters for watermelon seeds were determined, achieving a relative error of 2.60% with a static friction coefficient of 0.716 between watermelon seeds, a rolling friction coefficient of 0.051, and a collision recovery coefficient of 0.787 between watermelon seeds and plexiglass.

4) The accuracy of the calibrated parameters was confirmed by examining five key size parameters and the ratio of the stacked cross-sectional area within the air suction precision watermelon seed metering device. The findings indicated that the relative discrepancies between the simulated and physical stacking tests were all below 7.65%, suggesting that the physical parameters of the watermelon seeds derived in this study are suitable for use in subsequent kinetic simulations and movement analyses. A comparative analysis of the qualified index for both actual and simulated scenarios showed errors consistently below 4.38%. These results substantiated the viability and efficacy of the modeling approach presented in this research. Consequently, this study

enhanced the particle mobility of watermelon seeds, effectively circumvented distortion issues arising from improper simulation parameter settings, and offered a benchmark for future discrete element simulations of seed metering devices.

Acknowledgements

The authors gratefully acknowledge the Key Research and Development Special Project of Henan (Grant No. 241111111300), the Major Scientific and Technological Special Project of Henan Province (Grant No.231100110200).

[References]

[1] Liu H J, Chen Y Q, Lin M, Bai X S, Deng C H, Pan J H, et al. Selection of superior varieties (Lines) of seed-watermelon based on growth period and economic yield. Xinjiang Agricultural Sciences, 2018; 55(3): 430–438. (in Chinese)

[2] Yang L, Li Z M, Zhang D X, Li C, Cui T, He X T. Design and test of the T-shaped hole of centrifugal high-speed maize precision seed metering device. Transactions of the CSAE, 2024; 40(7): 50–60. (in Chinese)

[3] Zang Y, Huang Z S, Qin W, He S Y, Qian C, Jiang Y C, et al. Design of hybrid rice air-suction single-seed metering device. Transactions of the CSAE, 2024; 40(6): 181–191. (in Chinese)

[4] Yuan F H, Yu H W, Wang L, Shi Y Y, Wang X C, Liu H. Parameter calibration and systematic test of a discrete element model (DEM) for compound fertilizer particles in a mechanized variable-rate application. Agronomy, 2023; 13(3): 706.

[5] Zhang B, Wang J Y, Yang X S, Chen B S. A DEM-MBD based method for regulating transfer flux in the supply and discharge of cane seed particles. Computers and Electronics in Agriculture, 2024; 218: 108732.

[6] Zhang S W, Zhang R Y, Chen T Y, Fu J, Yuan H F. Calibration of simulation parameters of Mung bean seeds using discrete element method and verification of seed-metering test. Transactions of the CSAM, 2022; 53(3): 71–79. (in Chinese)

[7] Barrios G K P, Tavares L M. A preliminary model of high pressure roll grinding using the discrete element method and multi-body dynamics coupling. International Journal of Mineral Processing, 2016; 156: 32–42.

[8] Ghodki B M, Patel M, Namdeo R, Carpenter G. Calibration of discrete element model parameters: soybeans. Computational Particle Mechanics, 2019; 6(1): 3–10.

[9] Coetzee C. Calibration of the discrete element method: strategies for spherical and non-spherical particles. Powder Technology, 2020; 364: 851–878.

[10] Liu C L, Wang Y L, Du X, Song J N, Wang J C, Zhang F Y. Filling performance analysis and verification of cell-belt rice precision seed-metering based on friction and repeated filling principle. Transactions of the CSAE, 2019; 35(4): 29–36. (in Chinese)

[11] Tang H, Guan T Y, Xu F D, Xu C S, Wang J W. Test on adsorption posture and seeding performance of the high-speed precision dual-chamber maize metering device based on the seed characteristics. Computers and Electronics in Agriculture, 2024; 216: 108471.

[12] Chen Z, Wassgren C, Veikle E, Ambrose K. Determination of material and interaction properties of maize and wheat kernels for DEM simulation. Biosystems Engineering, 2020; 195: 208–226.

[13] Wang J W, Tang H, Wang J F, Li X, Huang H N. Optimization design and experiment on ripple surface type pickup finger of precision maize seed metering device. Int J Agric & Biol Eng, 2017; 10(1): 61–71.

[14] Wu J S, Cao C M, Xie C J, Fang L F, Wu Z M, Hu M K, et al. Measurement of physical properties of peucedani radix seeds and parameter calibration of discrete element simulation model. Journal of Gansu Agricultural University, 2019; 54(4): 180–189. (in Chinese)

[15] Su Y, Xu Y, Cui T, Gao X J, Xia G Y, Li Y B, et al. Determination and interpretation of bonded-particle model parameters for simulation of maize kernels. Biosystems Engineering, 2021; 210: 193–205.

[16] Wang Y X, Liang Z J, Zhang D X, Cui T, Shi S, Li K H, et al. Calibration method of contact characteristic parameters for corn seeds based on EDEM. Transactions of the CSAE, 2016; 32(22): 36–42. (in Chinese)

[17] Li Y X, Li F X, Xu X M, Shen C P, Meng K P, Chen J, et al. Parameter calibration of wheat flour for discrete element method simulation based on particle scaling. Transactions of the CSAE, 2019; 35(16): 320–327. (in Chinese)

[18] Lu C Y, Gao Z, Li H W, He J, Wang Q J, Wei X Y, et al. An ellipsoid modelling method for discrete element simulation of wheat seeds. Biosystems Engineering, 2023; 226: 1–15.

[19] Liu L, Wang X L, Zhang X C, Zhong X K, Wei Z C, Geng Y L, et al. Determination and verification of parameters for the discrete element modelling of single disc covering of flexible straw with soil. Biosystems Engineering, 2023; 233: 151–167.

[20] Peng Q J, He X, Li G M, Yang R S, Wang X Y, Zhang C Y, et al. Calibrating and testing the discrete element parameters for peanut seedling film. Int J Agric & Biol Eng, 2024; 17(5): 65–72.

[21] Khatchatourian O A, Binelo M O, de Lima R F. Simulation of soya bean flow in mixed-flow dryers using DEM. Biosystems Engineering, 2014; 123: 68–76.

[22] Li Y Z, Xie J H, Zhang J, Yue Y, Meng Q H, Du Y K, et al. Parameter calibration and experimental verification of discrete element simulation model for Protaetia brevitarsis larvae bioconversion mixture. Int J Agric & Biol Eng, 2024; 17(4): 35–44.

[23] Xie K T, Zhang Z G, Wang F A, Yu X L, Wang C L, Jiang S F. Calibration and experimental verification of discrete element parameters of Panax notoginseng root. Int J Agric & Biol Eng, 2024; 17(4): 13–23.

[24] Zhang Z G, Zeng C, Xing Z Y, Xu P, Guo Q F, Shi R M, et al. Discrete element modeling and parameter calibration of safflower biomechanical properties. Int J Agric & Biol Eng, 2024; 17(2): 37–46.

[25] Fan J F, Wang H W, Sun K, Zhang L, Wang L, Zhao J W, et al. Experimental verification and simulation analysis of a multi-sphere modelling approach for wheat seed particles based on the discrete element method. Biosystems Engineering, 2024; 245: 135–151.

[26] Zhao Z, Wu Y F, Yin J J, Tang Z. Monitoring method of rice seeds mass in vibrating tray for vacuum-panel precision seeder. Computers and Electronics in Agriculture, 2015; 114: 25–31.

[27] Ding X T, Wang B B, He Z, Shi Y G, Li K, Cui Y J, et al. Fast and precise DEM parameter calibration for *Cucurbita ficifolia* seeds. Biosystems Engineering, 2023; 236: 258–276.

[28] Aela P, Zong L, Esmaeili M, Siahkouhi M, Jing G Q. Angle of repose in the numerical modeling of ballast particles focusing on particle-dependent specifications: parametric study. Particuology, 2022; 65: 39–50.

[29] Chen Y, Gao X X, Jin X, Ma X R, Hu B, Zhang X L. Calibration and analysis of seeding parameters of Cyperus esculentus seeds based on discrete element simulation. Transactions of the CSAM, 2023; 54(12): 58–69. (in Chinese)

[30] Mousaviraad M, Tekeste M Z, Rosentrater K A. Calibration and validation of a discrete element model of corn using grain flow simulation in a commercial screw grain auger. Transactions of the ASABE, 2017; 60(4): 1403–1415.

[31] Zhong J Q, Tao L M, Li S P, Zhang B, Wang J Y, He Y L. Determination and interpretation of parameters of double-bud sugarcane model based on discrete element. Computers and Electronics in Agriculture, 2022; 203: 107428.

[32] Yuan J B, Li H, Wu C Y, Qi X D, Shi X X, Li C. Study on apace particle modeling of rice grain basis on the discrete element method. Journal of Nanjing Agricultural University, 2018; 41(6): 1151–1158. (in Chinese)

[33] Zhang R F, Jiao W, Zhou J L, Qi B, Liu H, Xia Q Q. Parameter calibration and experiment of rice seeds discrete element model with different filling particle radius. Transactions of the CSAM, 2020; 51(S1): 227–235. (in Chinese)

[34] Shi L R, Sun W, Zhao W Y, Yang X P, Feng B. Parameter determination and validation of discrete element model of seed potato mechanical seeding. Transactions of the CSAE, 2018; 34(6): 35–42. (in Chinese)